Available online at www.sciencedirect.com
ScienceDirect
Journal of the Mechanics and Physics of Solids 56 (2008) 1609–1623
JOURNAL OF THE MECHANICS AND PHYSICS OF SOLIDS
www.elsevier.com/locate/jmps

Internal lattice relaxation of single-layer graphene under in-plane deformation

Jun Zhou, Rui Huang*

Department of Aerospace Engineering and Engineering Mechanics, University of Texas, Austin, TX 78712, USA

Received 17 April 2007; received in revised form 12 July 2007; accepted 18 July 2007

Abstract

For noncentrosymmetric crystals, internal lattice relaxation must be considered for theoretical predictions of elastic properties. This paper develops a molecular dynamics approach for determination of the internal relaxation displacement in a single-layer graphene sheet under macroscopically homogeneous in-plane deformation. Based on an analytical interatomic potential, a generally nonlinear relationship between the internal relaxation displacement and the applied macroscopic strain is obtained explicitly from molecular dynamics simulations with a rhombic unit cell under finite deformation. A linear relationship is derived for relatively small strains, which can be conveniently incorporated into a continuum description of the elastic behavior of graphene. It is found that the internal relaxation has a strong effect on theoretical elastic moduli of graphene. In addition, the relationship between elastic properties for graphene and carbon nanotubes is discussed.

Keywords: Graphene; Carbon nanotube; Molecular dynamics; Elastic modulus

1. Introduction

A single-wall carbon nanotube (SWCNT) can be considered as rolled up from a planar graphene sheet, with a specific chirality and a nanoscale radius (Saito et al., 1998). The interests in carbon nanotubes for various applications continue to grow since their discovery (Iijima, 1991). In particular, mechanical properties of carbon nanotubes have been a focus of extensive studies, both experimentally and theoretically. Recently, planar graphene sheets have also attracted tremendous interest for their unusual electron transport properties (Novoselov et al., 2004; Berger et al., 2004; Y. Zhang et al., 2005; Stankovich et al., 2006). Little attention has been paid to mechanical properties of planar graphene sheets. However, the ultimate use of graphene sheets in integrated devices will likely require understanding of the mechanical properties that may affect the device performance and reliability as well as the intriguing morphology (Geim and Novoselov, 2007; Meyer et al., 2007; Van den Brink, 2007). One typically assumes that the in-plane elastic moduli of a single-layer graphene are identical to those for the base plane of hexagonal crystal graphite. However, significant discrepancies have

*Corresponding author. Tel.: +1 512 471 7558; fax: +1 512 471 5500.
E-mail address: ruihuang@mail.utexas.edu (R. Huang).

0022-5096/$ - see front matter © 2007 Elsevier Ltd. All rights reserved.
doi:10.1016/j.jmps.2007.07.013

been reported between theoretical predictions for in-plane Young's modulus and Poisson's ratio of graphene and those derived from graphite (Arroyo and Belytschko, 2004). It has also been noted that bending of a graphene sheet of a single atomic layer cannot be simply modeled using continuum plate or shell theories (Arroyo and Belytschko, 2004; Huang et al., 2006). Further studies are thus necessary in order to develop a theoretically consistent understanding for the mechanical properties of graphene as well as their relationships with corresponding properties of carbon nanotubes.

A theoretical approach is developed in the present study to predict the in-plane elastic properties of single-layer graphene based on an analytical interatomic potential. While similar approaches have been developed previously (e.g., Zhang et al., 2002; Arroyo and Belytschko, 2004), we herein emphasize the internal lattice relaxation under macroscopically homogeneous deformation and its effect on the elastic properties. In general, the method of homogeneous deformation provides a link between atomistic interactions and macroscopic elastic properties of crystals (Born and Huang, 1954). The Cauchy–Born rule maps an undeformed lattice to a deformed one by assuming homogeneous deformation at the atomic scale. This, however, requires the crystal lattice to be centrosymmetric so that internal equilibrium is maintained at every lattice point after deformation. For non-centrosymmetric crystals, it has been established that the relative displacement of sublattices leads to internal strain and inner elastic constants that must be accounted for in theoretical predictions of macroscopic properties (Martin, 1975; Cousins, 1978; Tadmor et al., 1999). The term, *internal relaxation*, literally reflects the fact that the internal displacement relaxes the potential energy from a homogeneously deformed lattice. The non-centrosymmetry in the graphene lattice has been noticed in recent studies of SWCNTs (e.g., Zhang et al., 2002; Arroyo and Belytschko, 2002, 2004; Jiang et al., 2003; H.W. Zhang et al., 2005). In these studies, the hexagonal lattice of graphene is decomposed into two simpler sublattices, each possessing centrosymmetry. The relative displacement between the sublattices is determined by minimizing the strain energy density under a macroscopic deformation. However, the general relationship between the internal displacement and the applied macroscopic strain has not been reported, with one exception in Huang et al. (2006) where a linear relationship was derived at the limit of infinitesimal deformation. As pointed out by Cousins (1978), the internal displacement not only contributes to the macroscopic elastic moduli but can also be directly related to experimental observables such as optical mode frequencies and scattering of X-rays or neutrons. The motivation of the present study is thus to obtain the internal displacement of graphene under generally finite deformation. This paper is organized as follows. Section 2 describes the theoretical approach combining a continuum mechanics description and a molecular dynamics (MD) method for the determination of internal relaxation. The results are presented in Section 3, with discussions on the effects of internal relaxation on elastic properties of both planar graphene and carbon nanotubes. Section 4 summarizes the findings.

2. Theory and method

Fig. 1 sketches a planar graphene lattice, with rhombic unit cells. Each unit cell (e.g., ABCD) contains two carbon atoms (P_1 and P_2), which replicates periodically in the directions parallel to the two base vectors, $\mathbf{b}_1$ and $\mathbf{b}_2$. While other types of unit cells have been used in previous studies, we find the rhombic cell to be most convenient for applying the periodic boundary condition in the study of elastic deformation, as will be described later.

2.1. Description of macroscopically homogeneous deformation

We describe a macroscopically homogeneous deformation by a constant displacement gradient tensor, namely,

$$\mathbf{H} = \nabla \mathbf{u}. \tag{1}$$

For the present study, only the two-dimensional (2D) in-plane displacements and their in-plane gradients are considered. In general, the displacement gradient is an asymmetric tensor, with four independent components for 2D deformation. Here we argue that, under the condition of rotational invariance, a symmetric displacement gradient tensor is sufficient for the description of arbitrary homogeneous deformation.

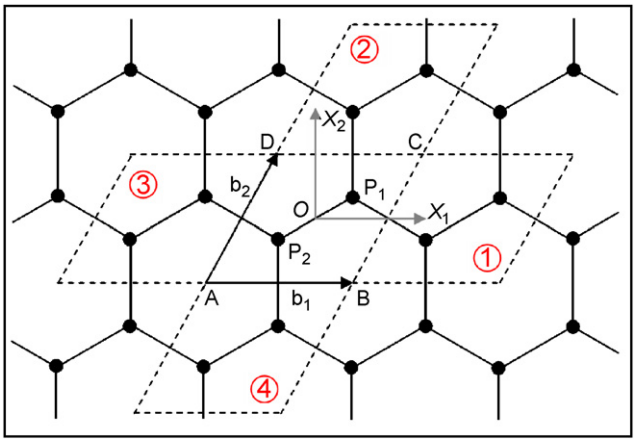

Fig. 1. Sketch of the hexagonal lattice of graphene, with the rhombic unit cell ABCD and four neighboring cells denoted by numbers 1–4.

In classical continuum mechanics (e.g., Marsden and Hughes, 1983; Fung and Tong, 2001), the deformation gradient, $\mathbf{F} = \mathbf{H} + \mathbf{I}$, maps an infinitesimal vector $d\mathbf{X}$ from a reference state to $d\mathbf{x}$ in a deformed state, i.e., $d\mathbf{x} = \mathbf{F}\,d\mathbf{X}$, where $\mathbf{I}$ is the identity tensor. An arbitrary deformation gradient can be decomposed into an orthogonal rotation tensor $\mathbf{R}$ and a symmetric stretch tensor $\mathbf{D}$ ($\mathbf{D}^{\mathrm{T}} = \mathbf{D}$) by the polar decomposition theorem, i.e., $\mathbf{F} = \mathbf{RD}$ or $\mathbf{F} = \mathbf{DR}$ (right or left polar decomposition, respectively). For a homogeneous deformation, $\mathbf{R}$ represents a rigid-body rotation. Since elasticity as a physical property of the material is invariant with respect to any rigid-body motion, we may arbitrarily set $\mathbf{R} = \mathbf{I}$ to exclude the rotation. As a result, the homogeneous deformation is fully described by the symmetric tensor $\mathbf{D}$. The corresponding displacement gradient, $\mathbf{H} = \mathbf{D} - \mathbf{I}$, is then symmetric too. Therefore, without loss of generality, any homogeneous deformation can be described by a symmetric displacement gradient tensor. It should be cautioned that this simplification cannot be applied to general inhomogeneous deformation where the rotation is not necessarily homogeneous throughout the body.

Incidentally, the symmetric displacement gradient is identical to the linear strain tensor,

$$\boldsymbol{\varepsilon} \equiv \tfrac{1}{2}(\mathbf{H} + \mathbf{H}^{\mathrm{T}}) = \mathbf{H}. \tag{2}$$

This simple relationship allows us to use the linear strain tensor as an engineering measure of arbitrary deformation, although it is typically used for infinitesimal deformation only. As will be shown later, the use of the linear strain tensor offers a numerically efficient procedure for both infinitesimal and finite deformation. The relationship between the linear strain and the Green–Lagrange strain is straightforward, namely,

$$\mathbf{E} = \boldsymbol{\varepsilon} + \tfrac{1}{2}\boldsymbol{\varepsilon}^2, \tag{3}$$

again under the condition of rotational invariance with $\mathbf{R} = \mathbf{I}$. While commonly used in the study of finite deformation, the nonlinear relationship makes it less convenient to directly apply the Green–Lagrange strain to the unit cell for the present study.

Now, using the symmetric displacement gradient tensor or equivalently, the linear strain tensor, we deform the rhombic unit cell of the graphene lattice by displacing its corners according to

$$\mathbf{u}_A = \mathbf{H}\mathbf{X}_A + \mathbf{u}_0, \tag{4}$$

where the subscript A refers to any one of the four corner points with $\mathbf{X}_A$ being its position vector before deformation, and $\mathbf{u}_0$ is the displacement of an arbitrarily selected point as the origin of the Cartesian coordinate. For convenience, we select the center of the unit cell (Point O in Fig. 1) as the origin and have the x_1-axis parallel to the base vector $\mathbf{b}_1$. For the central unit cell under consideration, we set $\mathbf{u}_0 = 0$ to exclude any rigid-body translation of the lattice. For each of the neighboring cells, the displacements of the corner points can be determined by using the same position vectors (relative to its own center) together with a translation

displacement by the periodic boundary condition, namely,

$$\mathbf{u}_A^{(i)} = \mathbf{H}\mathbf{X}_A + \mathbf{H}\mathbf{b}^{(i)}, \tag{5}$$

where $\mathbf{b}^{(i)}$ is the translation vector from the reference unit cell to the neighbor cell i, with $i = 1$–4 as denoted in Fig. 1. It can be seen that $\mathbf{b}^{(1)} = \mathbf{b_1}$, $\mathbf{b}^{(2)} = \mathbf{b_2}$, $\mathbf{b}^{(3)} = -\mathbf{b_1}$, and $\mathbf{b}^{(4)} = -\mathbf{b_2}$. Such a periodic replication of the deformed unit cell renders the entire graphene lattice under a macroscopically homogeneous deformation with a constant strain, $\boldsymbol{\varepsilon} = \mathbf{H}$.

2.2. Internal relaxation

While the deformation of the unit cells can be fully described by the macroscopic strain, the displacements of individual atoms do not necessarily follow the same rule. In fact, the corner points of each unit cell do not represent any physical atoms; they merely define the geometry of a virtual frame for the atoms before and after deformation, essentially a continuum description without concerning the discrete nature of the atomic structure inside the cells. Should the deformation maintain homogeneity down to the atomic scale within each unit cell, the displacements of individual atoms could be determined in the same manner, i.e., $\mathbf{u}_P = \mathbf{H}\mathbf{X}_P$ for the two atoms in the reference unit cell (P_1 and P_2), and $\mathbf{u}_P^{(i)} = \mathbf{H}\mathbf{X}_P + \mathbf{H}\mathbf{b}^{(i)}$ for the atoms in the neighboring cells. This would lead to deformed interatomic bonds, with changes in both the bond lengths and the bond angles in general. However, in such a homogeneously deformed lattice, internal equilibrium may not be maintained for each individual atom. In other words, the interatomic forces acting on each atom may not be balanced after such a deformation. A simple thought experiment may be instructive: applying a uniaxial strain ε_{11} to the unit cell, as illustrated in Fig. 2(a), would stretch the tilted bonds and change the bond angles, while the length of the vertical bond would remain unchanged by assuming homogeneous deformation within the unit cell. After such a deformation, the interatomic forces acting on each atom are balanced in the horizontal direction, but not necessarily so in the vertical direction. Depending on the specific interatomic interactions, whether two-body or many-body, the internal equilibrium must be maintained by allowing vertical displacements of the atoms that lead to stretching of the vertical bond, as illustrated in Fig. 2(b). Meanwhile, the overall shape of the deformed unit cell remains the same as in Fig. 2(a); thus, the deformation is still considered homogeneous at the macroscopic scale. From an energetic point of view, the internal displacements of the atoms relax the total potential energy without altering the macroscopic deformation. Therefore, the total displacement of each atom in general can be

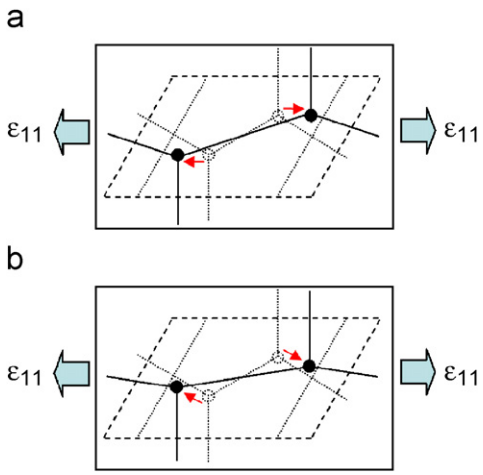

Fig. 2. Illustration of a uniaxially strained unit cell: (a) without internal relaxation, the atoms are only displaced in the horizontal direction; (b) with internal relaxation, the two atoms in the unit cell have a relative vertical displacement in addition to the horizontal displacement.

written as

$$\mathbf{u}_P = \mathbf{H}\mathbf{X}_P + \mathbf{u}_R, \tag{6}$$

where $\mathbf{u}_R$ is the internal relaxation displacement in addition to the macroscopic term, $\mathbf{H}\mathbf{X}_P$.

In early studies of crystal elasticity (e.g., Martin, 1975; Cousins, 1978), the internal displacement was defined as the relative displacement between centrosymmetric sublattices of non-centrosymmetric crystals. This idea has been followed in the previous studies of SWCNTs (e.g., Zhang et al., 2002; Arroyo and Belytschko, 2002, 2004; Jiang et al., 2003; H.W. Zhang et al., 2005), where two sublattices of graphene have been identified and the internal displacement was determined by an energy minimization approach. Here, we develop a MD approach to directly determine the internal displacement as a function of the macroscopic strain, which will be shown to be equivalent to the energy minimization approach but with advantages in numerical implementation for generally finite deformation.

2.3. Molecular dynamics (MD) simulation

Now we describe a mini-scale MD approach to determine the internal displacement under macroscopically homogeneous deformation. First, the unit cell is deformed according to Eq. (4), with a symmetric displacement gradient $\mathbf{H}$ or equivalently, a linear strain $\boldsymbol{\varepsilon}$ noting the relation in Eq. (2). The atoms in the deformed unit cell are displaced accordingly by Eq. (6), with $\mathbf{u}_R = \mathbf{0}$ as the initial condition. Then, the MD simulation starts by calculating the interatomic forces acting on each atom and updating their positions (i.e., $\mathbf{x}_P = \mathbf{X}_P + \mathbf{u}_P$) by the velocity Verlet algorithm (Swope et al., 1982; Haile, 1992). During the MD simulation, the base vectors of the deformed unit cell are fixed as $(\mathbf{I}+\mathbf{H})\mathbf{b}_{1,2}$. The deformed base vectors are used to determine the atomic positions in the neighboring cells by the periodic boundary condition, i.e., $\mathbf{x}_P^{(i)} = \mathbf{x}_P + (\mathbf{I}+\mathbf{H})\mathbf{b}^{(i)}$. Therefore, the macroscopic strain to the entire lattice remains constant during the MD simulation while the atoms search for their equilibrium positions. Ideally, a static molecular mechanics analysis would be sufficient for the search of the equilibrium positions. However, with generally nonlinear interatomic interactions, the implementation of a static analysis is not necessarily trivial. On the other hand, the implementation of the MD simulation is straightforward. Since the rhombic unit cell contains only two atoms, the MD simulation is computationally inexpensive.

The MD approach presented here is in fact equivalent to the energy minimization method used in the previous studies (Zhang et al., 2002; Arroyo and Belytschko, 2002, 2004; Jiang et al., 2003; H.W. Zhang et al., 2005) by two aspects. First, the two atoms in the rhombic unit cell, respectively, belong to the two sublattices used for energy minimization. Thus, the relative displacement of the two atoms within one unit cell is indeed the relative displacement between the two sublattices. Second, by the principle of thermodynamics, the internal equilibrium of the atoms is established at a state of minimum potential energy. The MD simulation described above is essentially a searching algorithm for the equilibrium positions of the atoms inside a deformed unit cell, which also minimize the potential energy under the imposed deformation. For this reason, no temperature control is involved in the MD simulation. A previous study (Jiang et al., 2005) developed a finite-temperature theory and showed that the elastic properties of graphene are insensitive to the temperature.

While the MD approach can be generally applied for any interatomic potentials, to be specific we use the Tersoff–Brenner potential (Tersoff, 1988; Brenner, 1990) for the carbon–carbon bond in graphene. The potential function is in the form of

$$V(r_{ij}) = V_R(r_{ij}) - \overline{B}_{ij} V_A(r_{ij}), \tag{7}$$

where r_{ij} is the distance between atom i and atom j, V_R and V_A are the repulsive and attractive terms, respectively, given by

$$\begin{aligned} V_R(r) &= \frac{D^{(e)}}{S-1} e^{-\sqrt{2S}\beta(r-R^{(e)})} f_c(r), \\ V_A(r) &= \frac{D^{(e)}S}{S-1} e^{-\sqrt{2/S}\beta(r-R^{(e)})} f_c(r), \end{aligned} \tag{8}$$

and f_c is a smooth cutoff function

$$f_c(r) = \begin{cases} 1, & r < R^{(1)}, \\ \frac{1}{2}\left(1 + \cos\left[\frac{(r - R^{(1)})\pi}{R^{(2)} - R^{(1)}}\right]\right), & R^{(1)} < r < R^{(2)}, \\ 0, & r > R^{(2)}. \end{cases} \tag{9}$$

In addition to the pair potential terms, the parameter $\overline{B}_{ij} = \frac{1}{2}(B_{ij} + B_{ji})$ accounts for the effect of bond angles that represents a multi-body interaction for the carbon–carbon bonds, and

$$B_{ij} = \left[1 + \sum_{k(\neq i,j)} G(\theta_{ijk}) f_c(r_{ik})\right]^{-\delta}, \tag{10}$$

where θ_{ijk} is the angle between bonds i–j and i–k, and the function G is given by

$$G(\theta) = a_0\left[1 + \frac{c_0^2}{d_0^2} - \frac{c_0^2}{d_0^2 + (1 + \cos\theta)^2}\right]. \tag{11}$$

The second set of the parameters for the interatomic potential given by Brenner (1990) is used in the MD simulations: $D^{(e)} = 6.000\,\text{eV}$, $R^{(e)} = 0.1390\,\text{nm}$, $\beta = 21\,\text{nm}^{-1}$, $S = 1.22$, $\delta = 0.50000$, $a_0 = 0.00020813$, $c_0 = 330$, and $d_0 = 3.5$. For a undeformed graphene sheet, these parameters lead to $\bar{B} = 0.9647$, and the equilibrium interatomic bond length, $r_0 = 0.145\,\text{nm}$, determined by minimizing the interatomic potential at the ground state. By using the cutoff radii $R^{(1)} = 0.17\,\text{nm}$ and $R^{(2)} = 0.20\,\text{nm}$ in Eq. (9), only the nearest neighbor atoms are included in the calculation of the potential. For a bond stretch less than $R^{(1)}/r_0 = 1.17$, the cutoff function $f_c \equiv 1$ for the nearest neighbor atoms.

As an example, Fig. 3 shows the result from a MD simulation with the unit cell subjected to a uniaxial strain $\varepsilon_{11} = 0.01$, as illustrated in Fig. 2. The two atoms are first displaced horizontally by $u_1 = \pm 0.0006279\,\text{nm}$ with $u_2 = 0$. At this point, the interatomic forces are balanced in the horizontal direction, while the unbalanced interatomic forces in the vertical direction move the atoms up and down. The vertical position of one atom (P_1 in Fig. 1) is plotted as a function of time in Fig. 3; the other atom in the unit cell moves symmetrically. Here, the mass of the carbon atom is taken to be 12 a.m.u. (atomic mass unit, i.e. $1.66 \times 10^{-27}\,\text{kg}$), and the time step for the MD simulation is 0.1 fs (i.e. $10^{-16}\,\text{s}$). The MD simulation naturally leads to oscillation of atoms, while the final equilibrium position of each atom can be determined as the average position that saturates over a sufficiently long period (e.g., 10 000–50 000 steps; see Figs. 3 and 5). Since the purpose of the MD simulation is to find the equilibrium atomic positions with the minimum potential energy, we are not

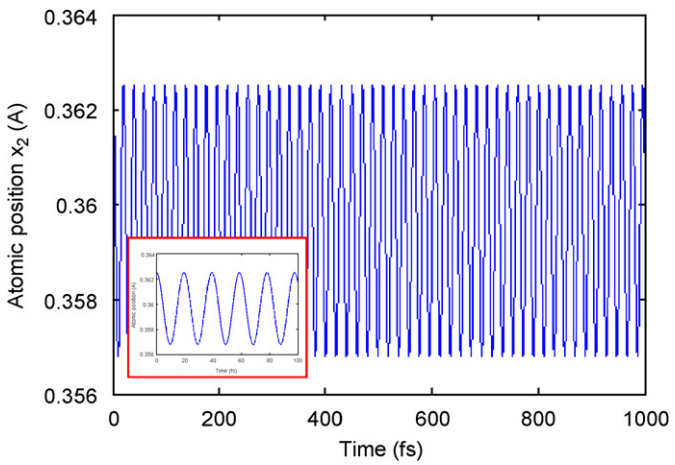

Fig. 3. Vertical position of atom P_1 in the unit cell under a uniaxial strain $\varepsilon_{11} = 0.01$ from a MD simulation. The inset shows the oscillation during the first 100 fs.

concerned with the kinetic energy of the atoms, or in the other words, the temperature effect is ignored. It can be seen from Fig. 3 that the atom oscillates like a linear spring, with a well-defined average position at $x_2 = 0.03596$ nm, where the potential energy is minimized. Compared to the initial position $x_2 = 0.03625$ nm, the internal relaxation leads to a vertical displacement, $u_2 = -0.00029$ nm, and an inner strain of 0.008 in the vertical direction, which is comparable to the applied macroscopic strain in the horizontal direction ($\varepsilon_{11} = 0.01$). The relative displacement between the two atoms in the unit cell (or equivalently, between the two sublattices) is then 0.00058 nm for the present case. Apparently, the internal displacement depends on the applied macroscopic strain as well as the specific interatomic potential used in the MD simulation. More results will be discussed in Section 3.

2.4. Theoretical elastic moduli

Once the internal displacement of each atom is determined by the MD simulations, the total potential energy of the unit cell can be calculated, which in general is a function of the macroscopic strain, i.e., $V_{\text{tot}}(\boldsymbol{\varepsilon})$. By the Cauchy–Born rule (Born and Huang, 1954), this potential energy equals the elastic strain energy. Thus, the elastic strain energy density (per unit area of the undeformed graphene sheet) is

$$U = \frac{V_{\text{tot}}(\boldsymbol{\varepsilon})}{\Omega_0}, \tag{12}$$

where $\Omega_0 = 3\sqrt{3}r_0^2/2$ is the area of the rhombic unit cell. Here, the linear strain tensor is used interchangeably with the symmetric displacement gradient by Eq. (2), without loss of generality for finite deformation under the condition of rotational invariance and macroscopically homogeneous deformation.

Within the general framework of hyperelasticity (Marsden and Hughes, 1983), the first Piola–Kirchhoff stress is defined as the work conjugate of the deformation gradient, which is, for the homogeneous deformation of graphene,

$$\mathbf{P} = \frac{\partial U}{\partial \mathbf{H}} = \frac{\partial U}{\partial \boldsymbol{\varepsilon}}. \tag{13}$$

Here, the use of the symmetric displacement gradient or the linear strain tensor gives a symmetric stress tensor in Eq. (13), although in general the first Piola–Kirchhoff stress is not symmetric. The true (Cauchy) stress, $\boldsymbol{\sigma}$, is related to the first Piola–Kirchhoff stress by

$$\boldsymbol{\sigma} = \frac{1}{J}\mathbf{P}\mathbf{D}^{\mathrm{T}} = \frac{1}{J}\mathbf{P}(\mathbf{I}+\boldsymbol{\varepsilon})^{\mathrm{T}}, \tag{14}$$

where $J = \det(\mathbf{I}+\boldsymbol{\varepsilon})$ is the Jacobian determinant. A tangent elastic modulus can then be defined as

$$\mathbf{C} = \frac{\partial \boldsymbol{\sigma}}{\partial \boldsymbol{\varepsilon}}. \tag{15}$$

Under an infinitesimal deformation, $J \approx 1$ and $\boldsymbol{\sigma} \approx \mathbf{P}$, thus

$$\mathbf{C} = \frac{\partial^2 U}{\partial \boldsymbol{\varepsilon}\partial \boldsymbol{\varepsilon}}. \tag{16}$$

Using the reduced notation for the fourth-order modulus tensor, we have

$$\begin{aligned} &C_{11} = \frac{\partial^2 U}{\partial \varepsilon_{11}^2}, \quad C_{22} = \frac{\partial^2 U}{\partial \varepsilon_{22}^2}, \quad C_{66} = \frac{\partial^2 U}{\partial \varepsilon_{12}^2}, \\ &C_{12} = \frac{\partial^2 U}{\partial \varepsilon_{11}\partial \varepsilon_{22}}, \quad C_{26} = \frac{\partial^2 U}{\partial \varepsilon_{22}\partial \varepsilon_{12}}, \quad C_{16} = \frac{\partial^2 U}{\partial \varepsilon_{11}\partial \varepsilon_{12}}, \end{aligned} \tag{17}$$

and the 2D in-plane stress–strain relation for the graphene can be written as

$$\begin{pmatrix} \sigma_{11} \\ \sigma_{22} \\ \sigma_{12} \end{pmatrix} = \begin{pmatrix} C_{11} & C_{12} & C_{16} \\ & C_{22} & C_{26} \\ \text{sym} & & C_{66} \end{pmatrix} \begin{pmatrix} \varepsilon_{11} \\ \varepsilon_{22} \\ 2\varepsilon_{12} \end{pmatrix}. \tag{18}$$

Note that all the partial differentiations in Eq. (17) should be taken at the undeformed state, i.e., $\boldsymbol{\varepsilon} = \mathbf{0}$, for the elastic moduli under infinitesimal deformation. Since no particular thickness is assumed for the single atomic layer of the graphene sheet, the unit for the stress as well as the elastic moduli is actually force per unit length (N/m) rather than force per unit area (N/m^2 or Pa). The ambiguity for the thickness of graphene and SWCNTs has been discussed in a previous study (Huang et al., 2006).

For general finite deformation, an incremental approach can be developed to determine the tangent modulus as a nonlinear function of the finite strain. For each increment, the linearized equation (16) can be used together with the currently deformed state as the reference configuration for the calculations of Ω_0 in Eq. (12) and the partial differentiations in Eq. (17). The details will be reported elsewhere (Zhou, 2007).

We note that, by combining the description of macroscopic deformation and the MD simulations, the present approach makes a direct link between continuum mechanics and an atomistic model. Evidently, for a single-layer planar graphene sheet under macroscopically homogeneous deformation, the continuum description is valid to the scale of a unit cell with two atoms, surprisingly close to the atomic scale, although an atomistic approach must be adopted for anything inside the unit cell. This, however, cannot be generalized to inhomogeneous deformation, where a much larger representative cell may have to be used and a mesoscopic description may be necessary to bridge macroscopic deformation and atomistic models (Tadmor et al., 1999; Arroyo and Belytschko, 2002).

3. Results and discussions

3.1. Internal relaxation displacements

Based on the general approach described in Section 2, MD simulations are conducted to determine the internal displacements of individual atoms in the unit cell of the graphene lattice subjected to macroscopically homogeneous in-plane deformation. Under the condition of rotational invariance, the symmetric displacement gradient or the linear strain tensor has three independent components. In general, the internal displacement nonlinearly depends on all the three components. For the convenience of discussion, we decompose the strain tensor into three basic deformation modes as follows:

$$\boldsymbol{\varepsilon} = \begin{bmatrix} \varepsilon_{11} & \varepsilon_{12} \\ \varepsilon_{21} & \varepsilon_{22} \end{bmatrix} = \varepsilon_{\mathrm{m}} \begin{bmatrix} 1 & 0 \\ 0 & 1 \end{bmatrix} + \varepsilon_{\mathrm{d}} \begin{bmatrix} 1 & 0 \\ 0 & -1 \end{bmatrix} + \varepsilon_{12} \begin{bmatrix} 0 & 1 \\ 1 & 0 \end{bmatrix}, \tag{19}$$

where $\varepsilon_{\mathrm{m}} = \frac{1}{2}(\varepsilon_{11} + \varepsilon_{22})$ and $\varepsilon_{\mathrm{d}} = \frac{1}{2}(\varepsilon_{11} - \varepsilon_{22})$.

The first term on the right-hand side of Eq. (19) represents an equi-biaxial deformation with the mean strain, and the other two terms correspond to two pure-shear modes (S1 and S2). It is found that, under an equi-biaxial deformation, i.e., $\varepsilon_{11} = \varepsilon_{22} = \varepsilon_{\mathrm{m}}$ and $\varepsilon_{12} = 0$, the atomic bonds in the graphene lattice undergo identical stretching in all directions with no distortion. In this case, the homogeneously deformed lattice maintains internal equilibrium without any internal relaxation; thus, $\mathbf{u}_{\mathrm{R}} = 0$ for arbitrary ε_{m}. This is in fact a special case where the continuum description of the homogeneous deformation is valid at the atomic scale, even for non-centrosymmetric lattices. Next we focus our attention on internal relaxation under the two shear deformation modes.

For deformation of the first shear mode (S1), i.e., $\varepsilon_{11} = \varepsilon_{\mathrm{d}}$, $\varepsilon_{22} = -\varepsilon_{\mathrm{d}}$, and $\varepsilon_{12} = 0$, it is found that the internal relaxation displacement is in the x_2-direction only, as the interatomic forces are always balanced in the x_1-direction under the biaxial deformation. MD simulations for mode S1 show similar atomic trajectory as that in Fig. 3, oscillating in the x_2-direction with the average position depending on the magnitude of ε_{d}. The internal displacement, u_{R2}, is determined by comparing the average position of the atom to its initial position upon homogeneous deformation, which is plotted in Fig. 4 for atom P_1 as a function of the strain ε_{d}; by

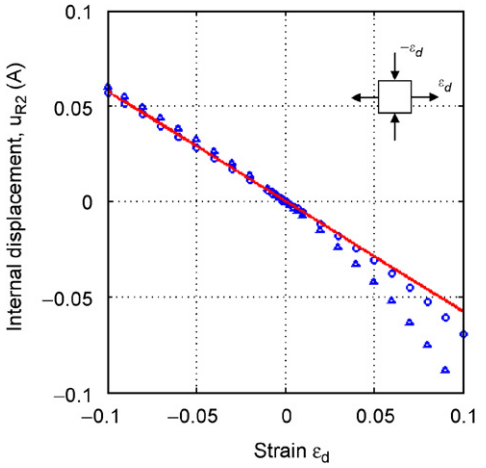

Fig. 4. Internal relaxation displacement of atom P_1 under mode-S1 deformation, with symbols △ from MD simulations neglecting the bond angle effect and symbols ○ from MD simulations including the bond angle effect. The solid straight line shows the linear fitting, $u_{R2} = -0.5777\varepsilon_d$ (Å), for small strains.

symmetry, the internal displacement for atom P_2 is simply $u_{R2}(P_2) = -u_{R2}(P_1)$. For comparison, the results from MD simulations neglecting the effect of bond angle by setting $\bar{B} = 0.9647$ as a constant are also plotted in Fig. 4. It is found that neglecting the bond–angle effect overestimates the internal displacement, especially for large deformation. The relationship between the internal displacement and the macroscopic strain is nonlinear in general and asymmetric for positive and negative ε_d. This is a reflection of the nonlinear nature of the interatomic potential, which is asymmetric for attraction and repulsion between two atoms. For small strains, a linear fitting of the MD results gives that

$$u_{R2} = -0.5777\varepsilon_d\,(\text{Å}), \tag{20}$$

which is a good approximation in the range $-0.1 < \varepsilon_d < 0.05$.

For the second shear mode (S2), i.e., $\varepsilon_m = \varepsilon_d = 0$, we find that the internal displacement is predominantly in the x_1-direction, while the relaxation in the x_2-direction is negligible for $-0.1 < \varepsilon_{12} < 0.1$. In this case, the atoms oscillate in both x_1 and x_2-directions. Fig. 5 shows the oscillation of atom P_1 in both directions under a shear strain, $\varepsilon_{12} = 0.01$. The average position in the x_1-direction has a shift from the initial position, while the shift in the x_2-direction is negligibly small. Fig. 6 compares the relaxation displacement u_{R1} as a function of the shear strain ε_{12} from the MD simulations with and without the bond angle effect. Again, neglecting the bond–angle effect overestimates the internal displacement. The relationship between the internal relaxation displacement and the macroscopic shear strain, while nonlinear in general, is symmetric with respect to the positive and negative shear strains. This is a reflection of the symmetry of the graphene lattice. For relatively small shear strains, a linear relationship can be obtained by fitting:

$$u_{R1} = -0.5779\varepsilon_{12}\,(\text{Å}), \tag{21}$$

which agrees well with the MD results in the range $-0.05 < \varepsilon_{12} < 0.05$.

It is noted that the coefficients in the linear relations (20) and (21) are nearly identical. Indeed, it can be shown theoretically that the six-fold symmetry of the hexagonal lattice requires identical coefficients in the linear relations for the two shear modes under small deformation. In essence, the relationship must remain invariant upon a rotation of $\pm 60^\circ$ for the lattice or the coordinates. This is independent of the specific interatomic potential used in the MD simulations, while the exact value for the coefficient does depend on the interatomic potential. The small difference between the coefficients in Eqs. (20) and (21) is believed to be numerical rather than physical. Incidentally, a recent study by Huang et al. (2006) derived an analytical formula for the internal relaxation under infinitesimal deformation, which predicts a coefficient of -0.5767 Å for the linear relations using the same interatomic potential; the agreement between the present MD results and the analytical solution is excellent in the linear regime. It should also be noted that, while internal

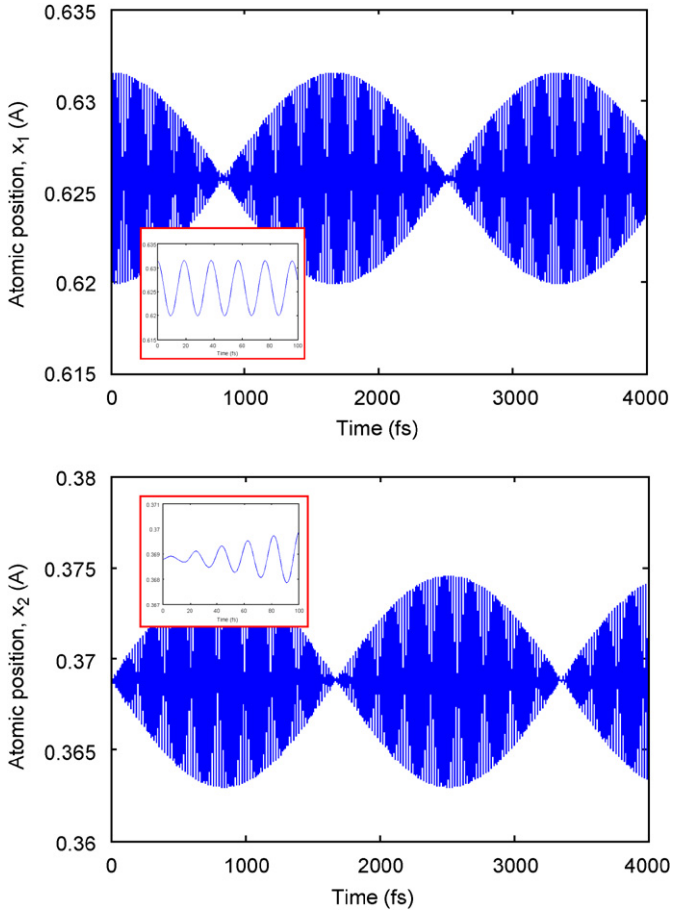

Fig. 5. Oscillation of atom P_1 in the unit cell under a shear strain $\varepsilon_{12} = 0.01$ from a MD simulation. The insets show the oscillation during the first 100 fs.

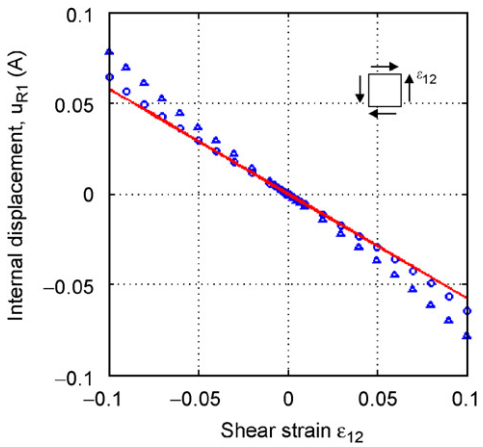

Fig. 6. Internal relaxation displacement of atom P_1 under mode-S2 deformation, with symbols △ from MD simulations neglecting the bond angle effect and symbols ○ from MD simulations including the bond angle effect. The solid straight line shows the linear fitting, $u_{R1} = -0.5779\varepsilon_{12}$ (Å), for small strains.

relaxation reflects underlying symmetry of the lattice, it is intrinsically anisotropic. This can be observed by comparing the internal displacements under pure shear deformation in different directions (modes S1 and S2 for two instances). On the other hand, as will be shown in the next section, the macroscopic elastic property of graphene is isotropic under infinitesimal in-plane deformation, despite the anisotropic internal relaxation.

Furthermore, although the internal relaxation under the three simple deformation modes in Eq. (19) can be analyzed separately, it should be noted that the internal relaxation under an arbitrary deformation in general cannot be simply obtained by linear superposition. Only in the range of small deformation, where the linear relationship between the internal displacement and the strain is applicable, should the linear superposition apply. As will be discussed in the next section, the linear relations are indeed sufficient for the prediction of theoretical elastic moduli under infinitesimal deformation. Nevertheless, the MD results as shown in Figs. 4 and 6 are valid for finite deformation under the simple deformation modes, and similar MD simulations can be carried out to determine the internal relaxation under arbitrary in-plane deformation.

3.2. Effect of internal relaxation on elastic moduli

For infinitesimal deformation, the in-plane elastic moduli in Eq. (18) are calculated under three different conditions for the purpose of comparison. First, the bond–angle effect is ignored by setting $\bar{B} = 0.9647$ as a constant and no internal relaxation is included in the calculation of the potential energy. This leads to a simple analytical result:

$$\mathbf{C}^{(1)} = C_0 \begin{pmatrix} 3 & 1 & 0 \\ 1 & 3 & 0 \\ 0 & 0 & 1 \end{pmatrix}, \tag{22}$$

where

$$C_0 = \frac{3r_0^2}{8\Omega_0}\left(\frac{\mathrm{d}^2 V_{\mathrm{R}}}{\mathrm{d}r^2} - \overline{B}\frac{\mathrm{d}^2 V_{\mathrm{A}}}{\mathrm{d}r^2}\right)_{r=r_0}. \tag{23}$$

Using the parameters listed in Section 2.3, we obtain $C_0 = 100.56\,\mathrm{N/m}$. The relationship among the moduli, i.e., $C_{11} - C_{12} = 2C_{66}$, implies isotropic in-plane elasticity. Under a uniaxial stress (actually force per unit length), the in-plane Young's modulus is $E^{(1)} = \frac{8}{3}C_0 = 268.17\,\mathrm{N/m}$, and the in-plane Poisson's ratio is $\nu^{(1)} = C_{12}/C_{11} = \frac{1}{3}$.

Next, including the multibody interaction through the bond–angle effect, still without considering internal relaxation, Eq. (16) leads to

$$\mathbf{C}^{(2)} = \mathbf{C}^{(1)} - \frac{1}{\Omega_0}\sum_{k=1}^{3}\left[2\frac{\partial \overline{B}^{(k)}}{\partial \boldsymbol{\varepsilon}}\frac{\partial V_{\mathrm{A}}^{(k)}}{\partial \boldsymbol{\varepsilon}} + V_{\mathrm{A}}(r_0)\frac{\partial^2 \overline{B}^{(k)}}{\partial \boldsymbol{\varepsilon}\partial \boldsymbol{\varepsilon}}\right]_{\boldsymbol{\varepsilon}=\mathbf{0}}, \tag{24}$$

where $k = 1$–3 for the three interatomic bonds in each unit cell. Using the same set of parameters for the interatomic potential, we now obtain that

$$\mathbf{C}^{(2)} = \begin{pmatrix} 347.25 & 54.99 & 0 \\ 54.99 & 347.25 & 0 \\ 0 & 0 & 146.13 \end{pmatrix} (\mathrm{N/m}). \tag{25}$$

Again, the elastic moduli are isotropic with $C_{11} - C_{12} = 2C_{66}$. But the in-plane Young's modulus $E^{(2)} = 338.54\,\mathrm{N/m}$ is higher than $E^{(1)}$, and the in-plane Poisson's ratio $\nu^{(2)} = 0.1584$ is now lower than $\nu^{(1)}$.

Finally, including both the bond–angle effect and the internal relaxation, we obtain that

$$\mathbf{C}^{(3)} = \mathbf{C}^{(2)} - \frac{l^2}{\Omega_0}\begin{pmatrix} C_2 & -C_2 & C_3 \\ -C_2 & C_2 & -C_3 \\ C_3 & -C_3 & C_1 \end{pmatrix}, \tag{26}$$

where $l=-0.5778\,\text{Å}$ is the average of the coefficients in the linear equations (20) and (21), and $C_1=\partial^2 V_{\text{tot}}/\partial u_{R1}^2$, $C_2=\frac{1}{4}\partial^2 V_{\text{tot}}/\partial u_{R2}^2$, $C_3=\frac{1}{2}\partial^2 V_{\text{tot}}/\partial u_{R1}\partial u_{R2}$. Since the total potential energy is a minimum at the zero strain, we have $C_1, C_2>0$ and $C_3=0$. Plugging in the parameters for the Tersoff–Brenner potential, we obtain that

$$\mathbf{C}^{(3)}=\begin{pmatrix}284.56 & 117.69 & 0\\ 117.69 & 284.56 & 0\\ 0 & 0 & 83.43\end{pmatrix}(\text{N/m}). \tag{27}$$

It turns out that $C_1\approx C_2$, which retains isotropy for the elastic moduli in Eq. (27). The internal relaxation, however, leads to a lower in-plane Young's modulus, $E^{(3)}=235.88\,\text{N/m}$, and a larger in-plane Poisson's ratios, $v^{(3)}=0.4136$.

Table 1 lists the in-plane Young's moduli and Poisson's ratios from the present study in comparison with other studies. Al-Jishi and Dresselhaus (1982) presented a lattice dynamics study of pristine graphite using a Born–von Karman model. They obtained both in-plane and out-of-plane elastic constants of graphite in good agreement with measured values. Under the condition of plane stress, the in-plane elastic constants for the base plane of the primitive graphite lattice derived from their results are

$$\mathbf{C}^{(4)}=\begin{pmatrix}353.0 & 58.2 & 0\\ 58.2 & 353.0 & 0\\ 0 & 0 & 147.4\end{pmatrix}(\text{N/m}). \tag{28}$$

Here, the interplane distance, 3.35 Å, for the graphite lattice is used to convert the bulk moduli (N/m^2) to the 2D in-plane moduli (N/m). The in-plane Young's modulus from Eq. (28) is: $E^{(4)}=343.4\,\text{N/m}$, and the in-plane Poisson's ratio is $v^{(4)}=0.165$. Apparently, these elastic moduli are in close agreement with Eq. (25), obtained from the present approach without consideration of internal relaxation. With internal relaxation, the elastic moduli in Eq. (27) from the present study show significant discrepancy with Eq. (28). However, this does not suggest that the internal relaxation should not be accounted for in the prediction of theoretical moduli. Rather, one possible cause for this discrepancy could be the use of the empirical Tersoff–Brenner potential and the fitted parameters. Using the same potential and parameters, Zhang et al. (2002) and Arroyo and Belytschko (2004) obtained the elastic moduli in close agreement with the present study, as listed in Table 1. Arroyo and Belytschko (2004) also reported that using the second-generation Brenner potential (Brenner et al., 2002) leads to little improvement. On the other hand, they found that, with slight adjustments to the parameters of the potential, the same approach predicts elastic moduli in close agreement with those derived from graphite as well as an *ab initio* study (Kudin et al., 2001). This demonstrates the necessity for further validation of the empirical potential and the fitting parameters used in many theoretical studies of

Table 1
Comparison of theoretical predictions for the in-plane Young's modulus and Poisson's ratio of a single-layer graphene sheet

	In-plane Young's modulus (N/m)	In-plane Poisson's ratio
Present study	268.17[a]	0.3333[a]
	338.54[b]	0.1584[b]
	235.88[c]	0.4136[c]
Arroyo and Belytschko (2004)	337.8[b]	0.1580[b]
	235.8[c]	0.4123[c]
Zhang et al. (2002)	236[c]	–
Al-Jishi and Dresselhaus (1982)	343.4[d]	0.165[d]
Kudin et al. (2001)	345[e]	0.149[e]

[a]No bond–angle effect and no internal relaxation.
[b]With bond–angle effect, but no internal relaxation.
[c]With bond–angle effect and internal relaxation.
[d]From a lattice dynamical model for graphite.
[e]From an *ab initio* model.

graphene and carbon nanotubes. Furthermore, it is noted that the lattice dynamics model by Al-Jishi and Dresselhaus (1982) included the interactions up to the fourth nearest in-plane neighbors, while the Tersoff–Brenner potential used in the present study includes only the first nearest neighbors. This suggests that a higher-order interatomic potential could be necessary to give consistent results from different approaches. Another possibly weak effect comes from the interlayer interactions in graphite, which may lead to physical difference between the in-plane elastic moduli for bulk graphite crystal and those for the single-layer graphene. This speculation, however, would have to be justified by experimental measurements or *ab initio* calculations for graphene.

3.3. On elastic properties of single-wall carbon nanotubes

From a planar sheet of single-layer graphene to a SWCNT, two effects on the elastic properties must be considered. First, as the graphene is bent into a small radius of curvature to form the SWCNT, the nonlinear elasticity of graphene under finite deformation leads to radius-dependent elastic properties in SWCNTs. As noted recently (Arroyo and Belytschko, 2004; Huang et al., 2006), the bending of graphene of a single atomic layer is conceptually different from bending of a continuum plate or shell. In particular, the bending stiffness of the graphene is not directly related to its in-plane stiffness since no particular thickness can be defined unambiguously for the single atomic layer. Instead, the bending stiffness results directly from the multibody interactions of carbon bonds, as included in the Tersoff–Brenner potential through the bond angle effect. Similar to the in-plane deformation considered in the present study, internal relaxation occurs under bending deformation. Theoretically, the 3D nature of the bending deformation requires both in-plane and out-of-plane internal relaxation. Interestingly, it was found that the out-of-plane internal relaxation is negligibly small for graphene subjected to bending (Y. Huang, private communication). Nevertheless, the bending deformation and associated internal relaxation define a specific ground state for each SWCNT, with the interatomic bonds and bond angles deformed from the planar graphene lattice. Consequently, the elastic moduli for a SWCNT, even under infinitesimal deformation relative to its ground state, are different from those for a planar graphene sheet. In terms of nonlinear elasticity or hyperelasticity as discussed in Section 2.4, the elastic moduli for a SWCNT are essentially the tangential moduli of the graphene under a finite bending deformation. As the tangential moduli in general vary nonlinearly with deformation, the elastic moduli of SWCNTs necessarily depend on the magnitude of the bending curvature, which is directly related to the tube radius, i.e., $\kappa = R^{-1}$. The smaller the tube radius, the larger is the bending deformation, and thus the stronger is the radius dependence of the elastic property. Many previous studies of SWCNTs have shown radius-dependent elastic moduli (e.g., Robertson et al., 1992; Yao and Lordi, 1998; Hernandez et al., 1998; Chang and Gao, 2003; Jiang et al., 2003; H.W. Zhang et al., 2005), while a few others showed otherwise (Lu, 1997; Jin and Yuan, 2003).

In addition to the radius dependence, the finite bending deformation of graphene can also lead to anisotropic elastic behavior in SWCNTs. Although the hexagonal lattice gives isotropic elastic behavior for graphene under infinitesimal deformation, a finite deformation, in-plane or bending, breaks the hexagonal symmetry. As a reflection of such anisotropy, the elastic moduli of SWCNTs would depend on the chirality (Robertson et al., 1992). Another interesting anisotropic phenomenon is the coupling between axial and shear deformation. Both stretch-induced torsion and the reverse coupling have been reported for SWCNTs (Gartstein et al., 2003; Liang and Upmanyu, 2006; Geng and Chang, 2006). As a physical consequence of nonlinear elasticity under finite deformation, it is not surprising that the coupling depends on both the radius and the chirality of SWCNTs. In fact, even for a planar graphene sheet, we found that the tangent elastic moduli become anisotropic under a finite in-plane deformation, with a nonzero coupling constants depending on the direction of axial deformation (Zhou, 2007). More quantitative understanding on the finite deformation induced nonlinear, anisotropic elastic behavior of graphene and carbon nanotubes is a subject for future studies.

4. Summary

To summarize, the present study develops a MD-based approach for the determination of the internal relaxation displacements in single-layer graphene under finite in-plane deformation. The relationships between

the internal relaxation and the macroscopic strain are obtained explicitly for simple deformation modes, based on the Tersoff–Brenner potential. While no internal relaxation under an equi-biaxial deformation, the two shear deformation modes lead to internal displacement in two perpendicular directions. Two linear relations are obtained for small deformation by fittings of the MD results. They are incorporated in the calculations of the potential energy for the prediction of elastic moduli of graphene under infinitesimal deformation. Finally, we emphasize the effect of multibody interaction and internal relaxation on the theoretical elastic moduli, and discuss the relationship between the elastic properties for graphene and SWCNTs.

Acknowledgments

This work is supported by National Science Foundation through Grant no. CMS-0547409. R.H. is grateful to Professor Yonggang Huang of University of Illinois at Urbana-Champaign for helpful discussions.

References

Al-Jishi, R., Dresselhaus, G., 1982. Lattice-dynamical model for graphite. Phys. Rev. B 26, 4514–4522.

Arroyo, M., Belytschko, T., 2002. An atomistic-based finite deformation membrane for single layer crystalline films. J. Mech. Phys. Solids 50, 1941–1977.

Arroyo, M., Belytschko, T., 2004. Finite crystal elasticity of carbon nanotubes based on the exponential Cauchy–Born rule. Phys. Rev. B 69, 115415.

Berger, C., Song, Z., Li, T., Li, X., Ogbazghi, A.Y., Feng, R., Dai, Z., Marchenkov, A.N., Conrad, E.H., First, P.N., de Heer, W.A., 2004. Ultrathin epitaxial graphite: 2D electron gas properties and a route toward graphene-based nanoelectronics. J. Phys. Chem. B 108, 19912–19916.

Born, M., Huang, K., 1954. Dynamical Theory of Crystal Lattices. Clarendon Press, Oxford.

Brenner, D.W., 1990. Empirical potential for hydrocarbons for use in simulating the chemical vapor deposition of diamond films. Phys. Rev. B 42, 9458–9471.

Brenner, D.W., Shenderova, O.A., Harrison, J.A., Stuart, S.J., Ni, B., Sinnott, S.B., 2002. A second-generation reactive empirical bond order (REBO) potential energy expression for hydrocarbon. J. Phys. Condens. Mater. 14, 783–802.

Chang, T., Gao, H., 2003. Size-dependent elastic properties of a single-walled carbon nanotube via a molecular mechanics model. J. Mech. Phys. Solids 51, 1059–1074.

Cousins, C.S.G., 1978. Inner elasticity. J. Phys. C: Solid State 11, 4867–4879.

Fung, Y.C., Tong, P., 2001. Classical and Computational Solid Mechanics. World Scientific, Singapore.

Gartstein, Y.N., Zakhidov, A.A., Baughman, R.H., 2003. Mechanical and electromechanical coupling in carbon nanotube distortions. Phys. Rev. B 68, 115415.

Geim, A.K., Novoselov, K.S., 2007. The rise of graphene. Nat. Mater. 6, 183–191.

Geng, J., Chang, T., 2006. Nonlinear stick-spiral model for predicting mechanical behavior of single-walled carbon nanotubes. Phys. Rev. B 74, 245428.

Haile, J.M., 1992. Molecular Dynamics Simulation: Elementary Methods. Wiley, New York.

Hernandez, E., Goze, C., Bernier, P., Rubio, A., 1998. Elastic properties of C and $B_xC_yN_z$ composite nanotubes. Phys. Rev. Lett. 80, 4502–4505.

Huang, Y., Wu, J., Hwang, K.C., 2006. Thickness of graphene and single-wall carbon nanotubes. Phys. Rev. B 74, 245413.

Iijima, S., 1991. Helical microtubules of graphitic carbon. Nature 354, 56–58.

Jiang, H., Zhang, P., Liu, B., Huang, Y., Geubelle, P.H., Gao, H., Hwang, K.C., 2003. The effect of nanotube radius on the constitutive model for carbon nanotubes. Comput. Mater. Sci. 28, 429–442.

Jiang, H., Huang, Y., Hwang, K.C., 2005. A finite-temperature continuum theory based on interatomic potentials. J. Eng. Mater. Technol. 127, 408–416.

Jin, Y., Yuan, F.G., 2003. Simulation of elastic properties of single-walled carbon nanotubes. Compos. Sci. Technol. 63, 1507–1515.

Kudin, K.N., Scuseria, G.E., Yakobson, B.I., 2001. C_2F, BN, and C nanoshell elasticity from ab initio computations. Phys. Rev. B 64, 235406.

Liang, H., Upmanyu, M., 2006. Axial–strain-induced torsion in single-walled carbon nanotubes. Phys. Rev. Lett. 96, 165501.

Lu, J.P., 1997. Elastic properties of carbon nanotubes and nanoropes. Phys. Rev. Lett. 79, 1297–1300.

Marsden, J.E., Hughes, T.J.R., 1983. Mathematical Foundations of Elasticity. Prentice-Hall, Englewood Cliffs, NJ.

Martin, J.W., 1975. Many-body forces in solids and the Brugger elastic constants: II. Inner elastic constants. J. Phys. C: Solid State Phys. 8, 2858–2868.

Meyer, J.C., Geim, A.K., Katsnelson, M.I., Novoselov, K.S., Booth, T.J., Roth, S., 2007. The structure of suspended graphene sheets. Nature 446, 60–63.

Novoselov, K.S., Geim, A.K., Morozov, S.V., Jiang, D., Zhang, Y., Dubonos, S.V., Grigorieva, I.V., Firsov, A.A., 2004. Electric field effect in atomically thin carbon films. Science 306, 666–669.

Robertson, D., Brenner, D.W., Mintmire, J.W., 1992. Energetics of nanoscale graphite tubules. Phys. Rev. B 45, 12592–12595.
Saito, R., Dresselhaus, G., Dresselhaus, M.S., 1998. Physical Properties of Carbon Nanotubes. Imperial College Press, London.
Stankovich, S., Dikin, D.A., Dommett, G.H.B., Kohlhass, K.M., Zimney, E.J., Stach, E.A., Piner, R.D., Nguyen, S.T., Ruoff, R.S., 2006. Graphene-based composite materials. Nature 442, 282–286.
Swope, W.C., Anderson, H.C., Berens, P.H., Wilson, K.R., 1982. A computer simulation method for the calculation of equilibrium constants for the formation of physical clusters of molecules: application to small water clusters. J. Chem. Phys. 76, 637–649.
Tadmor, E.B., Smith, G.S., Bernstein, N., Kaxiras, E., 1999. Mixed finite element and atomistic formulation for complex crystals. Phys. Rev. B 59, 235–245.
Tersoff, J., 1988. New empirical approach for the structure and energy of covalent systems. Phys. Rev. B 37, 6991–7000.
Van den Brink, J., 2007. Graphene: from strength to strength. Nature Nanotechnology 5, 199–201.
Yao, N., Lordi, V., 1998. Young's modulus of single-walled carbon nanotubes. J. Appl. Phys. 84, 1939–1943.
Zhang, H.W., Wang, J.B., Guo, X., 2005. Predicting the elastic properties of single-walled carbon nanotubes. J. Mech. Phys. Solids 53, 1929–1950.
Zhang, P., Huang, Y., Geubelle, P.H., Klein, P.A., Hwang, K.C., 2002. The elastic modulus of single-wall carbon nanotubes: a continuum analysis incorporating interatomic potentials. Int. J. Solids Struct. 39, 3893–3906.
Zhang, Y., Tan, Y.-W., Stormer, H.L., Kim, P., 2005. Experimental observation of the quantum Hall effect and Berry's phase in graphene. Nature 438, 201–204.
Zhou, J., 2007. Nonlinear and anisotropic elasticity for single-layer graphene and carbon nanotubes. Master's Thesis, The University of Texas, Austin.